NIH Public Access
Author Manuscript
Comput Methods Biomech Biomed Engin. Author manuscript; available in PMC 2014 April 01.

Published in final edited form as:
Comput Methods Biomech Biomed Engin. 2013 April ; 16(4): 451–462. doi:
10.1080/10255842.2011.627560.

Stabilization of walking by intrinsic muscle properties revealed in a three-dimensional muscle-driven simulation

Chand T. John[1], **Frank C. Anderson**[2], **Jill S. Higginson**[3], and **Scott L. Delp**[2,4]

Chand T. John: ctj@stanford.edu; Frank C. Anderson: clay.anderson@kinkaid.org; Jill S. Higginson: higginso@udel.edu; Scott L. Delp: delp@stanford.edu

[1]Department of Computer Science, Clark Center, Room S-324, Stanford University, Mail Code 5449, 318 Campus Drive, Stanford, CA 94305-5449, USA. Tel.: +1-650-725-1952. Fax: +1-650-724-1922

[2]Department of Bioengineering, Clark Center, Room S-321, Stanford University, Mail Code 5450, 318 Campus Drive, Stanford, CA 94305-5450, USA. Tel: +1-650-723-1230. Fax: +1-650-724-1922

[3]Department of Mechanical Engineering, 201A Spencer Laboratory, University of Delaware, Newark, DE 19716, USA. Tel: +1-302-831-6622. Fax: +1-302-831-3619

[4]Department of Mechanical Engineering, Clark Center, Room S-321, Stanford University, Mail Code 5450, 318 Campus Drive, Stanford, CA 94305-5450, USA. Tel: +1-650-723-1230. Fax: +1-650-723-8544

Abstract

A fundamental question in movement science is how humans perform stable movements in the presence of disturbances such as contact with objects. It remains unclear how the nervous system, with delayed responses to disturbances, maintains stability of complex movements. We hypothesized that intrinsic muscle properties (i.e., the force-length-velocity properties of muscle fibers and tendon elasticity) may help stabilize human walking by responding instantaneously to a disturbance and providing forces that help maintain the movement trajectory. To investigate this issue we generated a three-dimensional muscle-driven simulation of walking and analyzed changes in the simulation's motion when a disturbance was applied to models with and without intrinsic muscle properties. Removing intrinsic properties reduced stability; this was true when the disturbing force was applied at a variety of times and in different directions. Thus, intrinsic muscle properties play a unique role in stabilizing walking, complementing the delayed response of the central nervous system.

Keywords

biomechanics; simulation; muscle; walking; stability

1. Introduction

Stable walking requires maintaining a repetitive motion and responding to disturbances that threaten the execution of that motion. Humans are able to maintain a repetitive walking motion in the presence of disturbances including variations in terrain and contact with

---

Correspondence to: Scott L. Delp, `delp@stanford.edu`.

Video S1. Video showing muscle activations and motion of the model in the three-dimensional simulation of ten gait cycles of walking analyzed in this paper: https://simtk.org/docman/view.php/55/783/10gc.avi objects. An important goal of movement science is to elucidate the mechanisms that enable stable locomotion.

One of the most intriguing unresolved questions in movement science is how the central nervous system maintains stable locomotion despite delayed feedback from sensors. Delays are detrimental to stability, yet humans and animals are able to generate a wide variety of stable movements even though conduction of neural signals incurs substantial time delays. Reflexes are important mechanisms that maintain movement stability, yet most reflex responses occur after a delay of approximately 40–100 ms (Brown and Loeb 2000; Kimura et al. 1994; Reis 1961; Roby-Brami and Bussel 1987; Schillings et al. 1999; Shahani and Young 1971).

Muscle forces may change with no delay in response to disturbances, before reflexes or other active control mechanisms can come into play (Brown and Loeb 2000). The force generated by a muscle depends not only on the pattern of activation arriving from the central nervous system, but also on the length and contraction velocity of the muscle's fibers (known as "force-length" and "force-velocity" properties). The dependence of tendon force on tendon length ("tendon elasticity") also affects muscle force. It has been thought that the nonlinear dependence of muscle forces on length and velocity might make the central nervous system's job more difficult, requiring mechanisms to compensate for these complexities (Dyhre-Poulsen et al. 1991). However, the intrinsic stiffness (dependence of force on length) and damping (dependence of force on velocity) of muscles may help stabilize movement trajectories (i.e., resist disturbances) without active control by the central nervous system. Thus, muscle properties may play an important role in stabilizing movement.

It has been difficult to examine the role of muscle stiffness and damping in stabilizing walking, in part, because the relationships between patterns of muscle activation, muscle lengths and velocities, and the resulting muscle forces are poorly understood. Experimental methods alone cannot elucidate these relationships because important variables, such as muscle forces and their dependence on length and velocity, are generally not measurable during movement. It is especially difficult to examine the effects of muscle stiffness and damping during complex movements that involve activation of many muscles and movement of many joints. A change in the force of a single muscle can affect the motions of many joints (Zajac and Gordon 1989), so even if muscle properties stabilize one joint in response to a disturbance, they could destabilize other joints. Thus, it has been challenging to examine the effects of intrinsic muscle properties in the context of complex three-dimensional movements such as walking.

Muscle-driven simulations are powerful tools for investigating control of human movement. Recent simulations of walking, for example, have enabled researchers to examine how muscle forces are developed and contribute to body-weight support, forward propulsion, and body segment motions (Anderson and Pandy 2001; Anderson and Pandy 2003; Anderson et al. 2004; Arnold et al. 2005; Goldberg et al. 2004; Higginson et al. 2006; Liu et al. 2006; Liu et al. 2008; Neptune et al. 2001; Neptune et al. 2004; Neptune et al. 2008). Muscle-driven simulations complement experimental approaches by enabling one to eliminate the dependence of muscle force on its length and velocity to examine the effects of these intrinsic muscle properties on the stability of walking.

We present here a three-dimensional muscle-driven simulation of human walking. We generated a simulation of a walking man using a model of human musculoskeletal dynamics driven by 92 muscle-tendon compartments (Delp et al. 1990). We verified the accuracy with which the simulation reproduced the motions, joint moments, and muscle activation patterns of human walking. We then analyzed this simulation to examine whether intrinsic muscle properties help stabilize the body during walking. The walking simulation and OpenSim (Delp et al. 2007), the software used to create and analyze it, are freely available at https://simtk.org/home/muscleprops (reviewers: the files will be made public when this manuscript is accepted for publication; a private link can be provided to the editor if the reviewers wish to examine these files) enabling others to reproduce, modify, and analyze this simulation. This study contributes an accurate physics-based simulation of human walking and reveals that intrinsic muscle properties help stabilize human walking.

2. Materials and Methods

We generated a muscle-driven simulation of walking as follows (Figure 1). In an experiment, we recorded the positions of a subject's body segments and the forces and moments with which his feet contacted a treadmill. We collected data from an unimpaired man (height 1.83 m, body mass 65.9 kg) walking at a self-selected speed (1.36 m/s) on a treadmill (Bertec Corporation, Columbus, OH, USA) with split belts (one belt for each foot). A force plate under each belt measured the force and moment each foot applied to the treadmill during the movement every 1/600 second. Fourty-nine reflective markers were placed on the subject. A six-camera system (Motion Analysis Corporation, Santa Rosa, CA, USA) recorded the positions of the markers every 1/60 second. We created a three-dimensional musculoskeletal model (Delp et al. 1990; Thelen and Anderson 2006) of the subject consisting of 12 rigid body segments, 19 degrees of freedom, and 92 muscle-tendon compartments. Of the 19 degrees of freedom, 16 are the joint angles (including three orientation angles of the pelvis) and the remaining three specify the position of the pelvis. Each degree of freedom (i.e., joint angle or pelvis position coordinate) is represented as a coordinate of the model.

We scaled the model with 49 markers to match the size and mass of the subject. We then removed eight markers from the subject. We computed joint angles for the model at every time frame for which marker data were recorded (i.e., every 1/60 second) that minimized the sum of squared distances between the remaining 41 markers on the subject and the corresponding markers on the model. We computed the forces and moments acting at the joints that drove the model to follow the motions we recorded (see Supporting Information, Inverse Dynamics). Two of the quantities computed in this inverse dynamics process, the residual force and moment acting on model's pelvis, are non-physical forces (Kuo 1998) that are typically ignored in inverse dynamics calculations. We reduced the magnitudes and averages of the residual force and moment by making small adjustments to the model's motion (e.g., 1–2 degrees, see Supporting Information, Improving Dynamic Consistency). Finally, we used the computed muscle control algorithm (Thelen and Anderson 2006) to compute muscle activations that, when transformed via intrinsic muscle properties into muscle forces, resulted in close agreement between the model's motion and the adjusted joint angles. The result was a three-dimensional muscle-driven simulation of the subject walking for ten complete gait cycles (supplemental Video S1).

After generating the simulation, we performed a forward dynamics analysis in which we positioned the model at an arbitrary time in the simulation and advanced the model using the muscle activations determined by computed muscle control, while we simultaneously applied a constant 400 N downward disturbance to the mass center of the model's pelvis for 50 ms. Since we expect reflexes to respond only after 40 ms and muscle force generation and excitation-contraction coupling to require at least another 10 ms (Zajac 1989), this 50 ms analysis represents the intrinsic human muscle response to a disturbance without the assistance of reflexes. We chose this force and time period so the impulse of the disturbance (20 Ns) would be comparable to the impulses applied (e.g., approximately 32 Ns) in experimental studies investigating human stability during platform perturbations (Mille et al. 2003). To account for changes in the ground reaction force due to the disturbance we included a spring-damper unit to apply a restoring force in response to any deviation in position or velocity of the foot from its position and velocity in the original simulation. The muscle forces in the model were allowed to vary due to effects of the intrinsic muscle properties, including fiber force-length and force-velocity properties and tendon elasticity (see Supporting Information, Muscle Model). We then removed the intrinsic properties of the model's muscles and re-ran this 50-ms forward dynamics analysis, but with the muscle forces from the undisturbed simulation. We then repeated these two forward dynamics analyses with the original model ("model (i)") and the model without intrinsic properties ("model (ii)") while applying 400 N disturbances in the forward, backward, upward, rightward, and leftward directions. Note that although we drove model (ii) with muscle forces originally generated using intrinsic muscle properties, our use of model (ii) in this analysis is appropriate. Our goal was to create a reference set of muscle forces exhibiting physiologic realism (by virtue of the muscle activations reproducing major features of typical muscle activity for walking), so we could compare how adjustments to these muscle forces by intrinsic muscle properties would affect the response of model (i) versus model (ii) to the disturbances. We compared the amount by which the model's motion diverged from the simulation (i.e., the simulation generated using computed muscle control) in each forward dynamics analysis. At the end of each 50-ms analysis, we computed the absolute value of the difference between each model coordinate's value in the forward dynamics analysis and the same coordinate's value in the simulation. These absolute values indicate the amount by which each coordinate deviated from its value in the simulation due to the applied disturbance. We measured the stabilizing effects of intrinsic muscle properties by comparing these deviations between the models with and without intrinsic muscle properties. We characterize motion A as more stable than motion B if a majority of the model's 19 coordinates deviates less in motion A from the original walking motion than in motion B and the RMS deviation of the coordinates in motion A is less than the RMS deviation in motion B. Note that we do not define a motion as stable or unstable; we only define one motion as being more stable or less stable than another motion with respect to a reference walking motion.

Running a forward dynamics analysis without a disturbance over 50 ms resulted in negligible deviation (e.g., 0.002 degree) from the simulation. This is important since driving a model using muscle activations without any feedback can result in accumulation of numerical error, which can lead to deviation in the model's motion. We also wished to determine whether the deviation we observed in any forward dynamics analysis with a disturbance was due to the disturbance or due to the accumulation of numerical error. In a forward dynamics analysis with no disturbance where the model did have intrinsic muscle properties, only after approximately two seconds of movement did enough numerical error accumulate to cause substantial deviation (e.g., 4 degrees on average) in the model's motion. This suggests that in the forward dynamics analysis with a disturbance, the deviation we observed was due to the disturbance and not due to the accumulation of numerical error.

3. Results

3.1 Evaluation of 3D Walking Simulation

The simulation closely followed the joint angles that were measured in the experiment (Figure S1), with a maximum root mean square (RMS) deviation over all joint angles of one degree (Table S1). The averaged joint angles from the simulation over the ten gait cycles are consistent with previous experimental measurements of walking motions (Kadaba et al. 1989; Kadaba et al. 1990; Murray et al. 1985). See Supporting Information for detailed quantitative comparisons.

The net moments generated by the simulated muscles about the hip, knee, and ankle joints closely match the moments computed (see Supporting Information, Inverse Dynamics) from the experimental data (Figure S2). The moments about the lumbar joint agree with values typically reported for walking (Figure S3).

Muscle activations generated by the computed muscle control algorithm include important features of experimentally measured electromyography (EMG) data (Figure 2). For example, gluteus maximus and vasti are active in early stance, gluteus medius is active in mid-stance, and soleus and gastrocnemius are active in late stance (Rose and Gamble 2006). However, the computed muscle control algorithm failed to activate muscles in anticipation of future events. For example, EMG recordings show that gluteus maximus, gluteus medius, and the vasti are active slightly before the stance phase in anticipation of contact of the foot with the ground. Instead, in the simulation these muscles only become active slightly after the stance phase begins. See Supporting Information for detailed comparisons.

3.2 Stabilizing Effects of Intrinsic Muscle Properties

The intrinsic properties of muscle played an important role in stabilization of walking. For example, when we applied a 400 N downward disturbance to the pelvis of the original musculoskeletal model, the right knee flexion angle deviated by 2.9 degrees from the simulation’s motion after 50 ms. When we removed the intrinsic properties from the model’s muscles, the right knee flexion angle deviated by 5.3 degrees (Figure 3).

Removing the intrinsic muscle properties increased deviations in the joint angles (Table 1). For instance, when we applied a 400 N downward disturbance to the pelvis of the model with intrinsic muscle properties, the sum of the deviations of the joint angles from the simulation’s motion after 50 ms was 14.8 degrees (RMS deviation over all joint angles was 1.1 degrees). When we removed the intrinsic muscle properties, the sum of the deviations was 55.8 degrees (RMS deviation was 3.6 degrees). Removing the intrinsic properties caused 18 out of 19 coordinates to deviate more from the simulation’s motion than when including the intrinsic properties. The remaining coordinate (right hip adduction angle) deviated less than when intrinsic properties were included, but only by 0.1 degree (Table S3).

The deviations of coordinates in the presence and absence of intrinsic muscle properties were similar regardless of the direction of the disturbance (Table 1). While the differences in deviations were slightly lower for fore-aft and mediolateral disturbances, deviations were consistently lower when intrinsic muscle properties were included than when intrinsic properties were absent regardless of the disturbance direction. For example, when a forward disturbance was applied, the sum of joint angle deviations after 50 ms was 14.7 degrees when intrinsic muscle properties were included, while the sum of deviations was 34.1 degrees without intrinsic muscle properties. When a rightward disturbance was applied, the sum of joint angle deviations was 9.1 degrees when intrinsic muscle properties were included, while the sum of deviations was 23.0 degrees when intrinsic properties were absent.

Our results did not depend substantially on the starting time of the 50-ms forward dynamics analyses. The analysis above was performed during the double support phase of walking, but our results remained valid for other phases of the gait cycle. To show this, we performed the same 50-ms forward dynamics analyses starting at several different phases (Figure S5) of the gait cycle and found that the deviations did not exhibit major changes when the analyses were started at different times (Table S4). The deviations are shown in Table 1, Figure 3, and Table S3.

The stabilizing effect of intrinsic muscle properties was present regardless of the magnitude of the disturbance. Table S5 shows that for smaller disturbances, such as 200 N and 100 N, the stabilizing effect of intrinsic muscle properties was still present, albeit with smaller joint angle deviations for both the model with intrinsic muscle properties and the model without intrinsic muscle properties.

4. Discussion

We have produced a three-dimensional muscle-driven simulation of human walking that accurately reproduced the joint angles, joint moments, and muscle activations typical of human walking. Analysis of the simulation revealed that, with a few exceptions (Table S3), the joint angles of the model deviated less in response to a disturbing force when the intrinsic properties of muscle were included in the model. These results support the hypothesis that intrinsic muscle properties play an important role in stabilizing walking by providing stabilizing forces before reflexes come into play.

Brown and Loeb (Brown and Loeb 2000) also noted that intrinsic muscle properties respond without delay to disturbances, before active control mechanisms can respond. Using a planar arm model with three segments and six muscles, they applied disturbing forces to the endpoint of the arm and found that intrinsic muscle properties were important in responding to disturbances. They coined the term “preflex” to refer to the pre-reflex response of intrinsic muscle properties to disturbances.

The results of previous studies and our analysis support the assertion that intrinsic muscle properties help stabilize human gait. Gerritsen et al. (Gerritsen et al. 1998) used a two-dimensional model of the human body to examine the roles of intrinsic muscle properties in stabilizing walking. They showed that the intrinsic force-velocity property of muscle fibers resists an impulsive downward disturbance applied to the mass center of the model’s trunk while the force-length property of muscle fibers resists increased gravity. However, Kuo (Kuo 1999) showed that corrective muscle forces are needed to stabilize mediolateral motion, which cannot be captured by the planar model of Gerritsen et al. (Gerritsen et al. 1998). Daley et al. (Daley et al. 2009) showed that intrinsic muscle properties play a major role in stabilizing the motion of a running guinea fowl. They noted that reflexes require 30–40 ms to respond to a disturbance and that the immediate response to a disturbance is due solely to intrinsic muscle properties. Yakovenko et al. (Yakovenko et al. 2004) used a planar bipedal model to show that the intrinsic stiffness of leg muscles activated by a pre-determined pattern with no sensory feedback can produce a stable walking motion. Higginson et al. (Higginson et al. 2006) showed that intrinsic muscle properties reduce abnormal knee motion due to equinus foot placement (i.e., abnormally high ankle plantarflexion) during walking using a planar bipedal model. Unlike these previous studies, however, our analysis used an anatomically accurate musculoskeletal model (Delp et al. 1990; Thelen and Anderson 2006) based on experimental measurements of muscle architecture (Friederich and Brand 1990; Wickiewicz et al. 1983) to show how intrinsic muscle properties influence walking stability in three dimensions in the presence of disturbances applied in a variety of directions, independent of the phase of the gait cycle.

A few muscles generated passive force in addition to active force, but overall the passive component produced only a small fraction of the total force applied by the muscles. For example, in the analysis with a 400 N downward disturbance applied for 50 ms, the average passive fiber force exerted by all muscles remained less than 3 N per muscle-tendon compartment, while the average total (tendon) force exerted by all muscles reached almost 96 N per muscle-tendon compartment. Thus, we infer that passive muscle forces play a small role compared to active muscle forces in stabilizing the body during walking.

We have presented a three-dimensional muscle-driven simulation that reproduced major features of unimpaired walking for ten gait cycles. Previous simulations of walking (e.g., (Anderson and Pandy 2001)), have enabled researchers to examine how muscles contribute to vertical support, forward propulsion, and leg motions (Anderson and Pandy 2003; Anderson et al. 2004; Arnold et al. 2005; Goldberg et al. 2004; Higginson et al. 2006; Liu et al. 2006; Liu et al. 2008; Neptune et al. 2001; Neptune et al. 2004; Neptune et al. 2008). However, these simulations have been shorter in duration, typically less than a gait cycle; in our study, we needed a simulation of more than two seconds of walking to separate the destabilizing effects of disturbing forces from the destabilizing effects of numerical error during forward dynamics analyses. Other simulations of longer-duration walking movements have not effectively been compared to experimental data in the literature (Hase et al. 2003; Taga 1995) or have not been driven by muscles (Raibert and Hodgins 1991). The simulation in this study accurately reproduced the subject’s motion and joint moments from the experiment. The computed muscle control algorithm reproduced some muscle activation patterns well, although it failed to produce anticipatory muscle activations known to occur in humans.

Our results should be interpreted in light of several limitations. First, our musculoskeletal model is inherently unstable to a certain extent: after two seconds in an open-loop forward dynamics analysis, the model begins to deviate from the simulation’s original trajectory due to the accumulation of numerical error (see Materials and Methods). However, the model’s motion deviates much more rapidly in the presence of a disturbing force (e.g., 400 N) applied over a small time scale (e.g., 50 ms). Thus, due to the large difference in time scale during which the model remains close to the original walking motion with and without a disturbance, we believe that our study accurately captures the effect of the disturbance on the model’s motion and that the coordinate deviations we measured in the presence of disturbances were not due to the accumulation of numerical error. Although our study does not measure the overall stability of a model, we do compare the deviations of each model from a reference motion to show that intrinsic muscle properties resist the deviation of a model from a typical walking movement due to disturbances applied in a variety of directions.

Second, the Hill-type muscles (Thelen 2003) used in this study include intrinsic force-length and force-velocity properties of muscle fibers and elasticity of tendon, but lack other intrinsic properties of real muscles that could influence stability. For example, Daley et al. (Daley et al. 2009) showed that after an unexpected drop in terrain, history-dependent changes in force production, not captured by Hill-type muscle models, played a role in stabilizing the motion of a running guinea fowl. Also, short-range muscle stiffness (Rack and Westbury 1974) causes muscles to resist lengthening with a sharp rise in stiffness at the beginning of a movement. While the inclusion of additional properties of muscles, such as short-range stiffness, may increase stabilization, we have shown that force-length-velocity properties of muscle fibers and tendon elasticity make important contributions to stability. Note that our study does not separate out the effects of force-length-velocity properties of fibers and tendon elasticity on stabilization. The effects of fiber-tendon interaction can have notable effects on muscle function (Roberts and Azizi 2010), although tendon elasticity plays a smaller role in walking than in running (Cavagna and Kaneko 1977). The precise effects of short-range stiffness, history-dependent force changes, and other properties on stability could be investigated in future studies.

Third, our results have been determined only based on one subject. In other subjects, we would expect some small differences in the magnitudes of joint angle deviations and muscle activations due to differences in quantities such as the sizes and walking speeds of the subjects, but these changes would not alter the conclusions of the study.

Finally, we did not explicitly simulate arm motion. External forces and moments applied to the model (see Supporting Information) are intended, in part, to represent the mechanical effects of arm motion. Additional work is needed to better understand how arm motion affects the stability of walking.

In general, it has not been possible to reproduce the results of biomechanical simulation studies because few studies have made available the software and models used to generate their simulations. Generating accurate simulations requires substantial effort and the lack of available simulations has severely limited the use of simulations to investigate a variety of fundamental questions related to control and coordination of walking. The simulation of ten complete gait cycles presented in this study is available for analysis in OpenSim, a freely available software system, so that others can reproduce our results and perform additional analyses (Delp et al. 2007). This simulation can serve as reference data for a variety of future studies of normal and pathological walking.

Supplementary Material

Refer to Web version on PubMed Central for supplementary material.

Acknowledgments

We thank Ayman Habib, Ajay Seth, Jeffrey Reinbolt, Peter Loan, Samuel Hamner, May Liu, Michael Schwartz, Allison Arnold, Darryl Thelen, and Melanie Fox for feedback and assistance. We also thank Eran Guendelman for processing motion capture data and scaling the musculoskeletal model used in this study and Yuri Ivanenko for providing the EMG data from Cappellini et al. (2006). This work was funded by the Achievement Rewards for College Scientists Foundation and by the National Institutes of Health through the Roadmap for Medical Research U54 GM072970, NIH R01 NS55380, NIH R01 HD033929, and NIH GM63495.

References

Anderson FC, Pandy MG. Dynamic optimization of human walking. J Biomech Eng. 2001; 123:381–390. [PubMed: 11601721]

Anderson FC, Pandy MG. Individual muscle contributions to support in normal walking. Gait Posture. 2003; 17:159–169. [PubMed: 12633777]

Anderson FC, Goldberg SR, Pandy MG, Delp SL. Contributions of muscle forces and toe-off kinematics to peak knee flexion during the swing phase of normal gait: an induced position analysis. J Biomech. 2004; 37:731–737. [PubMed: 15047002]

Arnold AS, Anderson FC, Pandy MG, Delp SL. Muscular contributions to hip and knee extension during the single limb stance phase of normal gait: a framework for investigating the causes of crouch gait. J Biomech. 2005; 38:2181–2189. [PubMed: 16154404]

Cappellini G, Ivanenko YP, Poppele RE, Lacquaniti F. Motor patterns in human walking and running. J Neurophysiol. 2006; 95:3426–3437. [PubMed: 16554517]

Cappozzo A, Leo T, Pedotti A. A general computing method for the analysis of human locomotion. J Biomech. 1975; 8:307–320. [PubMed: 1184602]

Cappozzo A. The forces and couples in the human trunk during level walking. J Biomech. 1983; 16:265–277. [PubMed: 6863342]

Cavagna GA, Kaneko M. Mechanical work and efficiency in level walking and running. J Physiol. 1977; 268:467–481. [PubMed: 874922]

Crowninshield RD, Johnston RC, Andrews JG, Brand RA. A biomechanical investigation of the human hip. J Biomech. 1978; 11:75–85. [PubMed: 659458]

Daley MA, Voloshina A, Biewener AA. The role of intrinsic muscle mechanics in the neuromuscular control of stable running in the guinea fowl. J Physiol. 2009; 587:2693–2707. [PubMed: 19359369]

Delp SL, Loan JP, Hoy MG, Zajac FE, Topp EL, Rosen JM. An interactive graphics-based model of the lower extremity to study orthopaedic surgical procedures. IEEE Trans Biomed Eng. 1990; 37:757–767. [PubMed: 2210784]

Delp SL, Anderson FC, Arnold AS, Loan P, Habib A, John CT, Guendelman E, Thelen DG. OpenSim: Open-source software to create and analyze dynamic simulations of movement. IEEE Trans Biomed Eng. 2007; 55:1940–1950. [PubMed: 18018689]

Dyhre-Poulsen P, Simonsen EB, Voigt M. Dynamic control of muscle stiffness and H reflex modulation during hopping and jumping in man. J Physiol. 1991; 437:287–304. [PubMed: 1890636]

Featherstone, R.; Orin, D. Robot dynamics: equations and algorithms. Proc IEEE Int Conf Robotics & Automation; 2000. p. 826-834.

Friederich JA, Brand RA. Muscle fiber architecture in the human lower limb. J Biomech. 1990; 23:91–95. [PubMed: 2307696]

Gareis H, Solomonow M, Baratta R, Best R, D'Ambrosia R. The isometric length-force models of nine different skeletal muscles. J Biomech. 1992; 25:903–916. [PubMed: 1639834]

Gerritsen KGM, van den Bogert AJ, Hulliger M, Zernicke RF. Intrinsic muscle properties facilitate locomotor control—a computer simulation study. Motor Control. 1998; 2:206–220. [PubMed: 9644290]

Goldberg SR, Anderson FC, Pandy MG, Delp SL. Muscles that influence knee flexion velocity in double support: implications for stiff-knee gait. J Biomech. 2004; 37:1189–1196. [PubMed: 15212924]

Hase K, Miyashita K, Ok S, Arakawa Y. Human gait simulation with a neuromusculoskeletal model and evolutionary computation. J Visual Comput Animat. 2003; 14:73–92.

Higginson JS, Zajac FE, Neptune RR, Kautz SA, Burgar CG, Delp SL. Effect of equinus foot placement and intrinsic muscle response on knee extension during stance. Gait Posture. 2006; 23:32–36. [PubMed: 16311192]

Higginson JS, Zajac FE, Neptune RR, Kautz SA, Delp SL. Muscle contributions to support during gait in an individual with post-stroke hemiparesis. J Biomech. 2006; 39:1769–1777. [PubMed: 16046223]

Kadaba MP, Ramakrishnan HK, Wootten ME, Gainey J, Gorton G, Cochran GVB. Repeatability of kinematic, kinetic, and electromyographic data in normal adult gait. J Orthop Res. 1989; 7:849–860. [PubMed: 2795325]

Kadaba MP, Ramakrishnan HK, Wootten ME. Measurement of lower extremity kinematics during level walking. J Orthop Res. 1990; 8:383–392. [PubMed: 2324857]

Kimura J, Daube J, Burke D, Hallett M, Cruccu G, Ongerboer de Visser BW, Yanagisawa N, Shimamura M, Rothwell J. Human reflexes and late responses. Report of an IFCN committee. Electroencephalogr Clin Neurophysiol. 1994; 90:393–403. [PubMed: 7515783]

Kuo AD. A least-squares estimation approach to improving the precision of inverse dynamics computations. J Biomech Eng. 1998; 120:148–159. [PubMed: 9675694]

Kuo AD. Stabilization of lateral motion in passive dynamic walking. Int J Robot Res. 1999; 18:917–930.

Liu MQ, Anderson FC, Pandy MG, Delp SL. Muscles that support the body also modulate forward progression during walking. J Biomech. 2006; 39:2623–2630. [PubMed: 16216251]

Liu MQ, Anderson FC, Schwartz MH, Delp SL. Muscle contributions to support and progression over a range of walking speeds. J Biomech. 2008; 41:3243–3252. [PubMed: 18822415]

Mille M-L, Rogers MW, Martinez K, Hedman LD, Johnson ME, Lord SR. Thresholds for inducing protective stepping responses to external perturbations of human standing. J Neurophysiol. 2003; 90:666–674. [PubMed: 12711707]

Murray MP, Spurr GB, Sepic SB, Gardner GM, Mollinger LA. Treadmill vs. floor walking: kinematics, electromyogram, and heart rate. J Appl Physiol. 1985; 59:87–91. [PubMed: 4030579]

Neptune RR, Kautz SA, Zajac FE. Contributions of the individual ankle plantar flexors to support, forward progression and swing initiation during walking. J Biomech. 2001; 34:1387–1398. [PubMed: 11672713]

Neptune RR, Zajac FE, Kautz SA. Muscle force redistributes segmental power for body progression during walking. Gait Posture. 2004; 19:194–205. [PubMed: 15013508]

Neptune RR, Sasaki K, Kautz SA. The effect of walking speed on muscle function and mechanical energetics. Gait Posture. 2008; 28:135–143. [PubMed: 18158246]

Patriarco AG, Mann RW, Simon SR, Mansour JM. An evaluation of the approaches of optimization models in the prediction of muscle forces during human gait. J Biomech. 1981; 14:513–525. [PubMed: 7276011]

Rack PMH, Westbury DR. The short range stiffness of active mammalian muscle and its effect on mechanical properties. J Physiol. 1974; 240:331–350. [PubMed: 4424163]

Raibert MH, Hodgins JK. Animation of dynamic legged locomotion. Computer Graphics. 1991; 25:349–358.

Reis DJ. The palmomental reflex: a fragment of a general nociceptive skin reflex: a physiological study in normal man. Arch Neurol. 1961; 4:486–498. [PubMed: 13740641]

Roberts TJ, Azizi E. The series-elastic shock absorber: tendons attenuate muscle power during eccentric actions. J Appl Physiol. 2010; 109:396–404. [PubMed: 20507964]

Roby-Brami A, Bussel B. Long-latency spinal reflex in man after flexor reflex afferent stimulation. Brain. 1987; 110:707–725. [PubMed: 3107749]

Schillings AM, Van Wezel BMH, Mulder T, Duysens J. Widespread short-latency stretch reflexes and their modulation during stumbling over obstacles. Brain Res. 1999; 816:480–486. [PubMed: 9878872]

Shahani BT, Young RR. Human flexor reflexes. J Neurol Neurosurg Psychiatry. 1971; 34:616–627. [PubMed: 5122389]

Taga G. A model of the neuro-musculo-skeletal system for human locomotion: I. Emergence of basic gait. Biol Cybern. 1995; 73:97–111. [PubMed: 7662771]

Thelen DG. Adjustment of muscle mechanics model parameters to simulate dynamic contractions in older adults. J Biomech Eng. 2003; 125:70–77. [PubMed: 12661198]

Thelen DG, Anderson FC. Using computed muscle control to generate forward dynamic simulations of human walking from experimental data. J Biomech. 2006; 39:1107–1115. [PubMed: 16023125]

Wickiewicz TL, Roy RR, Powell PL, Edgerton VR. Muscle architecture of the human lower limb. Clin Orthop Relat Res. 1983; 179:275–283. [PubMed: 6617027]

Yakovenko S, Gritsenko V, Prochazka A. Contribution of stretch reflexes to locomotor control: a modeling study. Biol Cybern. 2004; 90:146–155. [PubMed: 14999481]

Zajac FE. Muscle and tendon: Properties, models, scaling, and application to biomechanics and motor control. Crit Rev Biomed Eng. 1989; 17:359–411. [PubMed: 2676342]

Zajac FE, Gordon ME. Determining muscle's force and action in multi-articular movement. Exerc Sport Sci Rev. 1989; 17:187–230. [PubMed: 2676547]

Appendix

Evaluation of the Motion of the Simulation

The average simulated pelvic tilt angle (i.e., the pelvic tilt angle during the simulation) was within one standard deviation of the values reported in Kadaba et al. (Kadaba et al. 1989). The average simulated pelvic list angle was within the range of values determined by the mean ± one standard deviation of the values reported by Kadaba et al. (Kadaba et al. 1989; Kadaba et al. 1990) for 56% of the gait cycle; the simulated angle deviated from Kadaba et al. (Kadaba et al. 1989) by at most 3.6 standard deviations. The average simulated pelvic rotation angle was within the range of values determined by the mean ± one standard deviation of the values reported by Kadaba et al. (Kadaba et al. 1989; Kadaba et al. 1990) for 77% of the gait cycle; the simulated angle deviated from Kadaba et al. (Kadaba et al. 1989) by at most 2.1 standard deviations. The average simulated right hip flexion angle remained within the range of values determined by the mean ± one standard deviation of the values reported by Kadaba et al. (Kadaba et al. 1989; Kadaba et al. 1990) for 100% of the gait cycle, while the left hip flexion angle did so for 98% of the gait cycle. The average simulated right hip adduction angle remained within the range of values determined by the mean ± one standard deviation of the values reported by Kadaba et al. (Kadaba et al. 1989; Kadaba et al. 1990) for 100% of the gait cycle, while the left hip adduction angle did so for 65.5% of the gait cycle; the simulated left hip adduction angle deviated from Kadaba et al. (Kadaba et al. 1990) by at most 1.8 standard deviations. The average simulated right hip rotation angle remained within the range of values determined by the mean ± one standard deviation of the values reported by Kadaba et al. (Kadaba et al. 1989; Kadaba et al. 1990) for 83% of the gait cycle, while the simulated left hip rotation angle did so for 71% of the gait cycle; the simulated right hip rotation angle deviated from Kadaba et al. (Kadaba et al. 1989) by at most 3.1 standard deviations, while the simulated left hip rotation angle deviated by at most 3.4 standard deviations. In the simulation, the knee did not fully extend in mid-stance (Figure S1), as was reported by Crowninshield et al. (Crowninshield et al. 1978); the average simulated right knee flexion angle deviated from Kadaba et al. (Kadaba et al. 1990) by at most 3.6 standard deviations, while the simulated left knee flexion angle did so by at most 2.6 standard deviations. The average simulated right ankle dorsiflexion angle deviated from Kadaba et al. (Kadaba et al. 1990) by at most 2.9 standard deviations, while the simulated left ankle dorsiflexion angle did so by at most 3.5 standard deviations.

Evaluation of the Joint Moments of the Simulation

Joint moments from the simulation generally agreed with hip flexion moments (Cappozzo et al. 1975; Crowninshield et al. 1978; Inman et al. 1981), hip adduction and rotation moments (Crowninshield et al. 1978; Patriarco et al. 1981), knee flexion and ankle plantarflexion moments (Cappozzo et al. 1975; Inman et al. 1981), and lower back moments (Cappozzo 1983) from the literature. A few differences between the simulated moments and literature are noted here. The hip flexion moment (Figure S2) in the simulation was higher in late stance than what has been reported in the literature. The hip flexion moment also reaches a maximum at an earlier time in the gait cycle than what has been reported in some sources (Cappozzo et al. 1975; Inman et al. 1981). However, the timing of the maximum hip flexion moment agrees well with Crowninshield et al. (Crowninshield et al. 1978). The knee extension moment (Figure S2) is low in push-off compared to the literature (Cappozzo et al. 1975; Patriarco et al. 1981), but the knee also did not extend fully from mid-stance through push-off, unlike typical literature values (see the section on Evaluation of the Motion of the Simulation). The ankle dorsiflexion moment (Figure S2) exhibits more dorsiflexion than typical literature values during early stance, but has a plantarflexion moment during late stance that agrees with the literature (Cappozzo et al. 1975; Patriarco et al. 1981). The lower back moments (Figure S3) generally agree with the literature (Cappozzo 1983).

Some asymmetry is apparent in the joint moments in this simulation. The hip abduction moment, hip rotation moment, and knee extension moment are at times higher on the left leg than on the right leg (Figure S2). However, the asymmetry in the knee extension moment did not appear to substantially affect the activation of the knee extensor muscles. Asymmetry in muscle activations is discussed further in the section below (Evaluation of the Muscle Activations of the Simulation).

Evaluation of the Muscle Activations of the Simulation

Gluteus maximus and gluteus medius activations patterns agreed with Perry (Perry 1992) and Cappellini et al. (Cappellini et al. 2006). The anterior compartment of the gluteus medius was activated not only during early stance, but also during late stance, which disagrees with Perry (Perry 1992) and Cappellini et al. (Cappellini et al. 2006), but is similar to activations modeled by Anderson and Pandy (Anderson and Pandy 2001). Iliacus, psoas, and tensor fasciae latae are activated during late stance. The activations of sartorius and tensor fasciae latae otherwise agree well with the literature.

The activations of muscles spanning the knee joint were slightly atypical, but were consistent with the joint moments in the simulation. Experimental electromyography (EMG) measurements (Cappellini et al. 2006; Perry 1992) demonstrate that the vasti become activated starting in terminal swing and remain activated through early stance. However, in our simulation, the vasti do not become activated until about 5–10% into each gait cycle, which is consistent with a knee extension moment not being generated until 5–10% into each gait cycle; this knee extension moment pattern is consistent with Cappozzo et al. (Cappozzo et al. 1975). The activations of the hamstrings muscles generally agree with the literature (Cappellini et al. 2006; Perry 1992), with semimembranosus and semitendinosus becoming activated in late swing and remaining activated through early stance. As reported in Perry (Perry 1992), the short head of the biceps femoris muscle becomes activated only in swing. Unlike what Perry (Perry 1992) reports, however, the rectus femoris muscle in our simulation does not exhibit a burst of activation in push-off (though it is slightly activated during push-off). This is consistent with the lower than normal knee flexion moment at push-off observed in this subject’s motion (see the section on Evaluation of the Motion of the Simulation).

Other muscles’ activations also agreed well with previous experimental studies. Plantarflexors (soleus and medial and lateral heads of gastrocnemius) and dorsiflexors (tibialis anterior, extensor hallucis longus, extensor digitorum longus) exhibit activations that are highly consistent with experimentally measured electromyography (EMG) (Cappellini et al. 2006; Perry 1992). Activations of hip abductor and adductor muscles generally agree with the literature (Cappellini et al. 2006; Perry 1992), although adductor magnus remains activated during part of the latter half of stance when there is a substantial hip abduction moment. There is some co-contraction between adductor magnus and hip abductors like sartorius and tensor fasciae latae during this time.

Asymmetry is evident in the activations of some muscles, similar to the asymmetry seen in some joint moments (see the section above on Evaluation of the Joint Moments of the Simulation). Gluteus medius, gluteus minimus, iliacus, and tensor fasciae latae on the left leg appear to have higher activations than do the corresponding muscles on the right leg.

Improving Dynamic Consistency

Typically, motion and ground reaction forces obtained from motion capture are dynamically inconsistent, i.e., they violate Newton’s Second Law, because of measurement error and modeling assumptions. When these motion and force data are fit to a musculoskeletal model of the human body via the inverse kinematics algorithm (described in the Materials and Methods section of the manuscript as computing joint angles for the model that minimized the sum of squared distances between the measured and model marker positions), the ground reaction forces and moments, inertia properties, and accelerations of the model thus violated Newton’s Second Law, so a nonzero residual force and a nonzero residual moment were applied to make the whole system satisfy Newton’s Second Law. However, since the residual force and moment were unphysiologic, a residual reduction algorithm (Delp et al. 2007) was used to make small changes to the location of the center of mass of the torso segment in the model, the total mass of the model, and the joint angles to reduce the magnitudes of the residual force and moment acting on the model during the movement.

The residual reduction algorithm modified the movement mechanics such that the lumbar (lower back) extension moment in the simulation agrees more closely with the literature than the moment computed from the experimental data (Figure S3).

The residual reduction algorithm modified the pelvis translations by 2 cm, 1 cm, and 1 cm (RMS) in the fore-aft, vertical, and mediolateral directions respectively (Table S2). The residual reduction algorithm reduced the amplitudes of the fore-aft, vertical, and mediolateral components of the residual force from 45 N to 6 N, from 134 N to 14 N, and from 43 N to 5 N, respectively, and the frontal component of the residual moment from 53 Nm to 29 Nm. The residual reduction algorithm changed the amplitudes of the transverse and sagittal components of the residual moment by less than 1 N, but the algorithm reduced the absolute values of the average values of the frontal and sagittal components from 7.1 Nm to 1.3 Nm and from 12.8 Nm to 0.3 Nm (Figure S4).

Deviations of 50-ms Simulations due to Disturbances

Table S4 shows 50-ms analyses we ran starting at times in the gait cycle other than the one we presented in the paper. Figure S5 shows the configuration of the model at each of these times. Start times and durations for these analyses are:

- Starting at 44% of the gait cycle (8.0 s): the 50-ms analysis runs from 77 to 27 ms before right initial contact, so the contact event is not included in the forward dynamics analysis.
- Starting at 80% of the gait cycle (8.4 s): the 50-ms analysis occurs during right single stance: it starts approximately 120 ms after left toe-off; no foot-ground contact event occurs during the forward dynamics analysis.
- Starting at 7% of the gait cycle (8.7 s): the 50-ms analysis occurs during the right-to-left double support phase starting 80 ms after left initial contact; no foot-ground contact event occurs during the forward dynamics analysis.

For smaller disturbing forces like 200 N and 100 N, we have observed results similar (but with smaller deviations in the joint angles) to those reported in the manuscript. When upward disturbances are applied, a 400 N disturbing force caused a RMS deviation of 4 degrees over all joint angles over 50 ms when intrinsic muscle properties were absent, as opposed to a 200 N disturbing force, which caused a RMS deviation of 1.9 degrees and a 100 N disturbing force, which caused a RMS deviation of 0.9 degree (Table S5).

Muscle Model

Each muscle-tendon compartment in our musculoskeletal model is represented by the muscle model described in this section. The muscle model used in our simulation is a slight modification of the Hill-type muscle model presented in (Thelen 2003). At a given time t in a simulation, the muscle model's inputs are activation, $a(t)$ (a real number between 0 and 1 inclusive), and fiber length, $l^M(t)$. The muscle model's outputs are the force, $F^{MT}(t)$, of the muscle-tendon compartment and, for the next time step, $t+\Delta t$, the time-derivative of activation, $\dot{a}(t+\Delta t)$, and the time-derivative of fiber length, $\dot{l}^M(t+\Delta t)$. Here we will describe how the force of the muscle-tendon compartment, time-derivative of activation, and fiber velocity are calculated.

Activation dynamics represents how an excitation, $u(t)$, a unit-less value between 0 and 1 is transformed into an activation, $a(t)$, a unit-less value between 0 and 1, of a muscle. When a muscle is neurally excited, its activation gradually increases, while if a muscle's excitation decreases, its activation also decreases, albeit at a slower rate than the increase. The time-derivative of activation is calculated as:

$$\dot{a}\ (t+\Delta t)=\begin{cases} (u(t)-a(t))/\tau_{act}, & u(t)\geq a(t) \\ (u(t)-a(t))/\tau_{deact}, & u(t)<a(t) \end{cases},$$

where τ_{act} = 10 ms and τ_{deact} = 40 ms.

As shown in Figure S6A, our muscle model consists of two parts: the muscle fibers and the tendon. The muscle fibers may be slanted relative to the tendon at an angle called the pennation angle. The muscle fibers consist of a passive element that produces passive force (i.e., force due to the fibers' inherent stiffness) and a contractile element that produces active force (i.e., force due to activation of the muscle).

Our muscle model contains several parameters. Some parameter values vary between muscles in our musculoskeletal model while other parameter values are the same for all muscles. The parameter values that vary between muscles are:

- F_0^M, the maximum isometric force of the muscle
- l_0^M, the optimal fiber length of the muscle
- l_s^T, the tendon slack length, the tendon length below which the tendon (and therefore the whole muscle) produces zero force
- α_0, the pennation angle of the muscle fibers at the optimal fiber length

The parameter values that are the same across muscles are:

- $\varepsilon_0^M=0.6$, passive muscle strain due to maximum isometric force
- k_{toe} = 3, an exponential shape factor
- $\varepsilon_0^T=0.033$, tendon strain due to maximum isometric force
- $k_{lin}=1.712/\varepsilon_0^T$, a linear shape factor
- $\varepsilon_{toe}^T=0.609\varepsilon_0^T$, tendon strain above which tendon force is linear with respect to tendon strain
- $\overline{F}_{toe}^T=0.333333$, normalized tendon force above which tendon force is linear with respect to tendon strain
- k^{PE}= 4, an exponential shape factor for the passive force-length relationship
- γ = 0.5, a shape factor for the Gaussian active force-length relationship
- A_f = 0.3, a shape factor for the force-velocity relationship
- $\overline{F}_{len}^M=1.8$, maximum normalized muscle force achievable when the fiber is lengthening

A bar over variables representing lengths indicates normalization with respect to the optimal fiber length, e.g., $\overline{l}^M=l^M/l_0^M$ is the "normalized fiber length." A bar over variables representing forces indicates normalization with respect to the maximum isometric force, e.g., $\overline{F}^{MT}=F^{MT}/F_0^M$ is the "normalized muscle-tendon compartment force."

The computation of muscle-tendon compartment force proceeds as follows. From the configuration of the musculoskeletal model of the body at time t, we obtain the length of the whole muscle-tendon unit, $l^{MT}(t)$. The tendon length is then calculated:

$$l^T(t)=l^{MT}(t)-l^M\cos\alpha(t).$$

From this, a normalized quantity called the tendon strain is calculated:

$$\varepsilon^T=(\bar{l}^T-\bar{l}_s^T)/\bar{l}_s^T.$$

Then the tendon force is calculated as $F^T(t)=F_0^M\overline{F}^T(\varepsilon^T)$, where

$$\overline{F}^T(\varepsilon^T)=0.001(1+\varepsilon^T)+\begin{cases} k_{lin}(\varepsilon^T-\varepsilon_{toe}^T)+\overline{F}_{toe}^T, & \varepsilon^T>\varepsilon_{toe}^T \\ \overline{F}_{toe}^T\frac{e^{k_{toe}\varepsilon^T/\varepsilon_{toe}^T}-1}{e^{k_{toe}}-1}, & 0<\varepsilon^T\le\varepsilon_{toe}^T \\ 0, & \varepsilon^T\le 0 \end{cases}$$

represents the normalized tendon force-strain relationship, also known as tendon elasticity, tendon compliance, or tendon stiffness. The extra term $0.001(1+\varepsilon^T)$ exists to prevent the tendon from going completely slack during a simulation. The tendon attaches the muscle fibers to the bones in the musculoskeletal model, so the force in the tendon is the force generated by the muscle-tendon compartment as a whole, so $F^{MT}(t) = F^T(t)$.

The computation of fiber velocity proceeds as follows. The width of each muscle, kept constant as $w=l_0^M\sin\alpha_0$, and the current fiber length, $l^M(t)$, are used to calculate the pennation angle

$$\alpha(t)=\begin{cases} 0, & l^M(t)=0\ or\ w/l^M(t)\le 0 \\ \sin^{-1}\left(w/l^M(t)\right), & 0<w/l^M(t)<1 \\ \pi/2, & w/l^M(t)\ge 1 \end{cases}.$$

The active force in the muscle fibers is computed as

$$F_a(t)=a(t)f_1\left(l^M(t)\right)=a(t)F_0^M\bar{f}_l\left(\bar{l}^M(t)\right),$$

where

$$\bar{f}_l\left(\bar{l}^M(t)\right)=e^{-\left(\bar{l}^M(t)-1\right)^2/\gamma}$$

is a Gaussian function representing the normalized active force-length relationship for all muscles in our musculoskeletal model. The passive force in the muscle fibers is computed as $F^{PE}(t)=F_0^M\overline{F}^{PE}\left(\bar{l}^M(t)\right)$, where

$$\overline{F}^{PE}\left(\bar{l}^M\right)=\begin{cases} 1+\frac{k^{PE}}{\varepsilon_0^M}\left(\bar{l}^M-\left(1+\varepsilon_0^M\right)\right), & \bar{l}^M>1+\varepsilon_0^M \\ \frac{e^{k^{PE}\left(\bar{l}^M-1\right)/\varepsilon_0^M}}{e^{k^{PE}}}, & \bar{l}^M\leq 1+\varepsilon_0^M \end{cases}$$

is a function representing the normalized passive force-length relationship for all muscles in our musculoskeletal model. This function is affine for large forces (the first case in the above equation) and is otherwise exponential (the second case in the equation). The total effect of the normalized passive and active force-length relationships yields a function that increases, levels off, decreases slightly, and then increases rapidly (Figure S6B). All muscles in our musculoskeletal model have this same normalized force-length property. It has been shown that the shape of the total force-length curve for different muscles in the body are not identical (Gareis et al. 1992): while some muscles have a slight decrease after the level portion of the total force-length curve, others have a significant decrease, and some have an increase instead of a decrease. Therefore, our model is an approximation of the total force-length relationships of muscles in real humans.

The force in the contractile element is then calculated as

$$F^{CE}(t)=\frac{F^T(t)}{\cos\alpha(t)}-F^{PE}(t).$$

The distinction between the force in the contractile element and the active force calculated above is that the active force does not include the effects of the force-velocity relationship of the muscle fibers. We calculate this force-velocity scale factor as

$$\overline{F}_V^M\left(\dot{\bar{l}}^M(t+\Delta t)\right)=\frac{F^{CE}(t)}{F_a(t)}.$$

$\overline{F}_V^M$ is an invertible function representing the normalized force-velocity relationship. The normalized fiber velocity is calculated as

$$\dot{\bar{l}}^M(t+\Delta t)=\left(\overline{F}_V^M\right)^{-1}\left(\frac{F^{CE}(t)}{F_a(t)}\right),$$

where, for any normalized force *f*,

$$\left(\overline{F}_V^M\right)^{-1}(f)=\begin{cases}\left(1+\frac{1}{A_f}\right)f-1, & f<0\\ \frac{f-1}{1+\frac{f}{A_f}}, & 0\le f<1\\ \frac{(f-1)\left(\overline{F}_{len}^M-1\right)}{\left(2+\frac{2}{A_f}\right)\left(\overline{F}_{len}^M-f\right)}, & 1\le f<0.95\overline{F}_{len}^M\\ \frac{10\left(\overline{F}_{len}^M-1\right)}{\left(1+\frac{1}{A_f}\right)\overline{F}_{len}^M}\left(-18.05\overline{F}_{len}^M+18+\frac{20f\left(\overline{F}_{len}^M-1\right)}{\overline{F}_{len}^M}\right), & 0.95\overline{F}_{len}^M\le f\end{cases}$$

The exact implementation of $\left(\overline{F}_V^M\right)^{-1}$ is slightly different to adjust for possible numerical issues as described below. The fiber velocity (un-normalized) is

$$\dot{l}^M(t+\Delta t)=V_{\max}\bar{\dot{l}}^M(t+\Delta t),$$

where

$$V_{\max}=(5+5a)l_0^M.$$

Note that $\bar{\dot{l}}^M$ is different from $\dot{\bar{l}}^M$. $\bar{\dot{l}}^M$, which we calculated above, is the fiber velocity normalized (i.e., divided) by V_{max}, while $\dot{\bar{l}}^M$ is the fiber velocity normalized (i.e., divided) by l_0^M:

$$\dot{\bar{l}}^M=\frac{d}{dt}\left[\bar{l}^M\right]=\frac{d}{dt}\left[\frac{l^M}{l_0^M}\right]=\frac{1}{l_0^M}\frac{d}{dt}\left[l^M\right]=\frac{\dot{l}^M}{l_0^M}.$$

The original normalized force-velocity relationship is

$$\overline{F}_V^M(v)=\begin{cases}\frac{v+1}{1+\frac{1}{A_f}}, & v<-1\\ \frac{v+1}{1-\frac{v}{A_f}}, & -1\le v<0\\ \frac{\left(2+\frac{2}{A_f}\right)v\overline{F}_{len}^M+\overline{F}_{len}^M-1}{\left(2+\frac{2}{A_f}\right)v+\overline{F}_{len}^M-1}, & 0\le v<\frac{10\left(\overline{F}_{len}^M-1\right)\left(0.95\overline{F}_{len}^M-1\right)}{\left(1+\frac{1}{A_f}\right)\overline{F}_{len}^M}\\ \frac{\overline{F}_{len}^M}{20\left(\overline{F}_{len}^M-1\right)}\left(\frac{\left(1+\frac{1}{A_f}\right)\overline{F}_{len}^M v}{10\left(\overline{F}_{len}^M-1\right)}+18.05\overline{F}_{len}^M-18\right), & \frac{10\left(\overline{F}_{len}^M-1\right)\left(0.95\overline{F}_{len}^M-1\right)}{\left(1+\frac{1}{A_f}\right)\overline{F}_{len}^M}\le v\end{cases}.$$

This function was inverted to obtain the expressions for $\left(\overline{F}_V^M\right)^{-1}$ above, but in the implementation, some additional constants, $\xi = 0.05$ (a passive damping factor for the force-velocity relationship) and $\varepsilon = 10^{-6}$ are incorporated to prevent possible numerical errors. The complete implementation of the inverted normalized force-velocity relationship is as follows.

$$\left(\overline{F}_{V}^{M}\right)^{-1}\left(F^{CE},F_a\right)=\begin{cases}\frac{F^{CE}}{\varepsilon}\left(\frac{\varepsilon-F_a}{F_a+\frac{\varepsilon}{A_f}+\xi}+\frac{F_a}{F_a+\xi}\right)-\frac{F_a}{F_a+\xi}, & F^{CE}<0\\ \frac{F^{CE}-F_a}{F_a+\frac{F^{CE}}{A_f}+\xi}, & 0\leq F^{CE}<F_a\\ \frac{F^{CE}-F_a}{\frac{\left(2+\frac{2}{A_f}\right)\left(F_a\overline{F}_{len}^{M}-F^{CE}\right)}{\overline{F}_{len}^{M}-1}+\xi}, & F_a\leq F^{CE}<0.95F_a\overline{F}_{len}^{M}\\ f_{v0}+\frac{F^{CE}-0.95F_a\overline{F}_{len}^{M}}{\varepsilon F_a\overline{F}_{len}^{M}}\left(f_{v1}-f_{v0}\right), & 0.95F_a\overline{F}_{len}^{M}\leq F^{CE}\end{cases},$$

where

$$f_{v0}=\frac{0.95F_a\overline{F}_{len}^{M}-F_a}{\frac{\left(2+\frac{2}{A_f}\right)0.05F_a\overline{F}_{len}^{M}}{\overline{F}_{len}^{M}-1}+\xi}$$

and

$$f_{v1}=\frac{(0.95+\varepsilon)F_a\overline{F}_{len}^{M}-F_a}{\frac{\left(2+\frac{2}{A_f}\right)(0.05-\varepsilon)F_a\overline{F}_{len}^{M}}{\overline{F}_{len}^{M}-1}+\xi}.$$

The curves representing the active force-length, passive force-length, and force-velocity properties of fibers and the elasticity of tendon are shown in Figure S6.

Inverse Dynamics

Forces and moments at the joints of the subject in this study were computed from experimental data using a process known as inverse dynamics (Featherstone and Orin 2000). Given a model and its motion (e.g., joint angles as functions of time), Newton's second law is applied to the rigid body segments in the model to compute the forces and moments required at the joints to drive the model to follow the given motion.

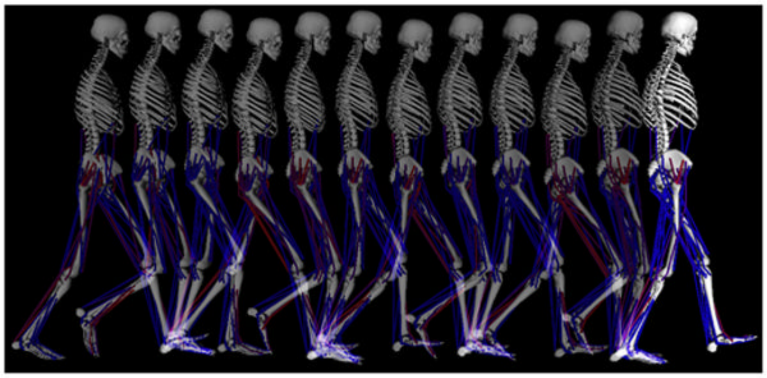

Figure 1.
Three-dimensional muscle-driven simulation of walking. The frames from the animation show the skeletal motion and muscle activation patterns (muscles with high activation are shown in red and muscles with low activation are shown in blue) for a portion of the simulation.

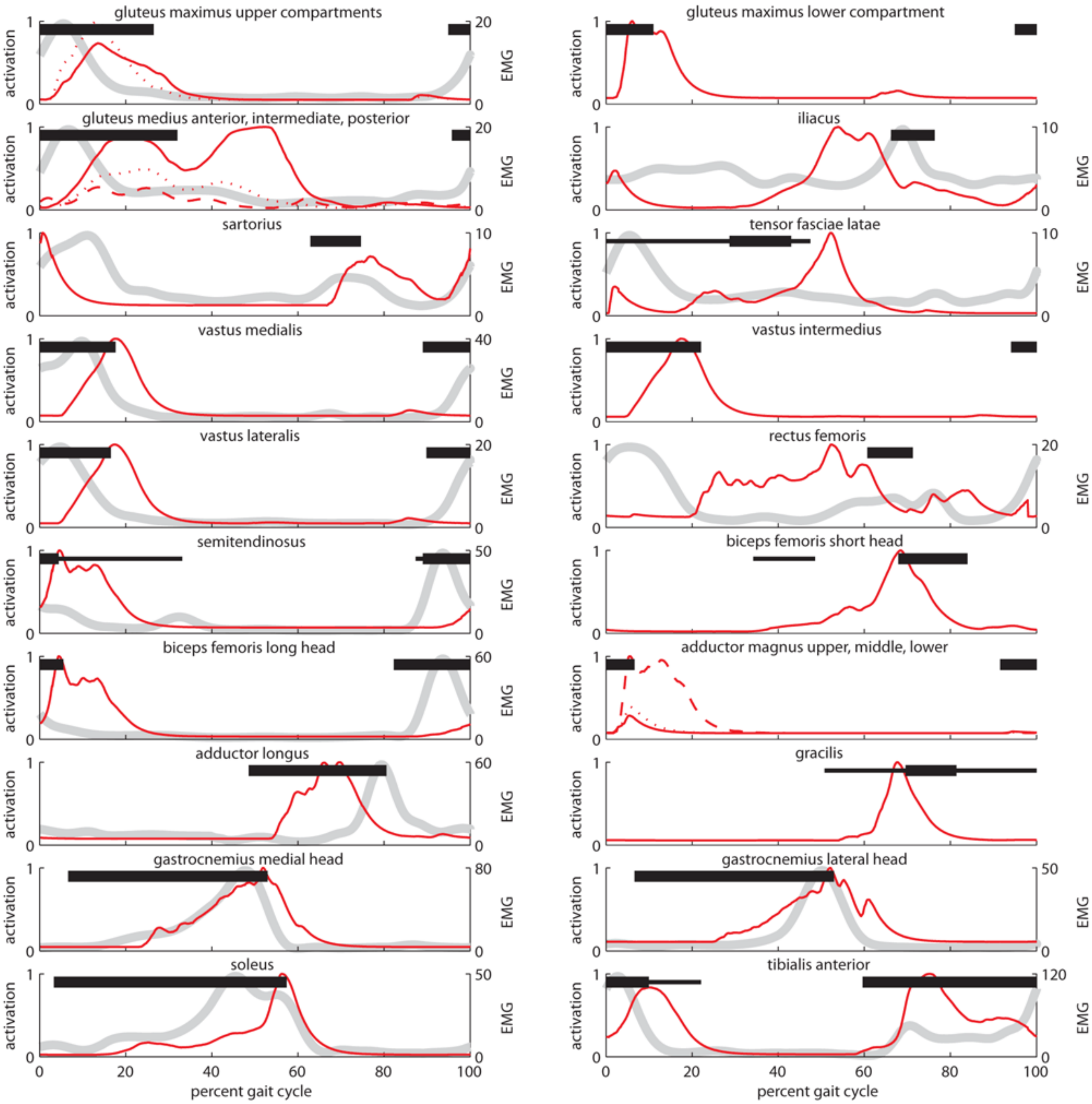

Figure 2.

Muscle activations vs. literature electromyography (EMG) data. The red curves represent the mean muscle activations from the simulation on a scale of 0 to 1, where 0 denotes no activation and 1 denotes the maximum mean activation of each muscle during the simulation, across ten gait cycles for the left leg. In any graph with multiple red curves, the solid curve represents the activation of the first muscle compartment, the dotted curve represents the second compartment, and the dashed curve represents the third compartment. The gray curve represents the EMG data in microvolts (μV) reported for adults walking at a comparable speed by Cappellini et al. (Cappellini et al. 2006). The maximum activation for each muscle was plotted at the same height as the maximum EMG value of the muscle reported by Cappellini et al. (Cappellini et al. 2006). The black bars represent the times during which a muscle is expected to be activated as reported by Perry (Perry 1992).

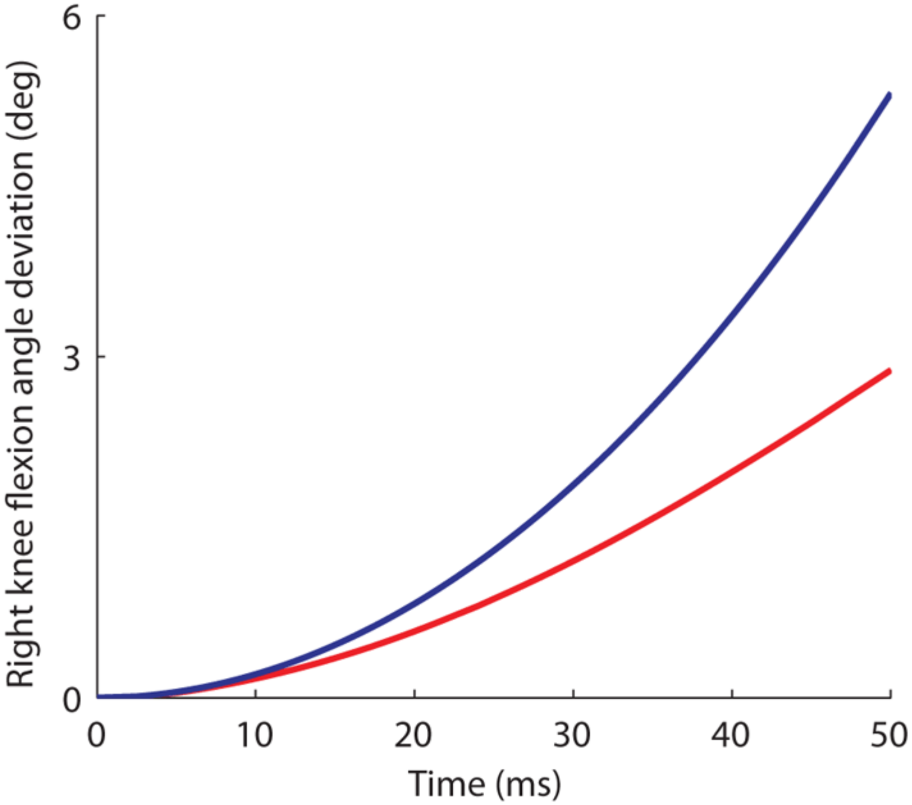

Figure 3.

Right knee flexion angle deviations vs. time during a disturbance. The red curve represents the deviation in knee flexion angle as a 400 N downward disturbance is applied to the mass center of the pelvis over a 50-ms period during the left-to-right double support phase; the model's muscles have intrinsic properties. The blue curve represents the deviation in knee flexion angle during the same disturbance, but with the muscles' intrinsic properties removed. The knee flexion angle deviates more from its values in the simulation when the muscles lack intrinsic properties.

Table 1

Deviations of model coordinates from the simulation after a 50-ms forward dynamics analysis with a 400 N disturbance applied throughout the 50 ms to the mass center of the pelvis.

	Forward	**Backward**	**Upward**	**Downward**	**Rightward**	**Leftward**
# worse (no props)	14/19	14/19	17/19	18/19	16/19	14/19
Sum (with props)	14.7	14.2	15.2	14.8	9.1	9.2
Sum (no props)	34.1	36.2	62.6	55.8	23.0	22.7
RMS (with props)	1.1	1.0	1.0	1.1	0.7	0.7
RMS (no props)	2.5	2.7	4.0	3.6	1.7	1.8

Deviations were computed for disturbances in six different directions: forward, backward, upward, downward, rightward, and leftward. The “# worse (no props)” row shows the number of coordinates (out of 19 total) for which the model with no intrinsic muscle properties deviates as much or more from the simulation than the model with all intrinsic muscle properties. The remaining four rows represent sums of deviations and RMS deviations of the 16 joint angles (including the three pelvis orientation angles) during forward dynamics analyses using the model with all intrinsic muscle properties “(with props)” and the model with no intrinsic muscle properties “(no props).” See Table S3 for the deviations of each model coordinate. This table pertains to the forward dynamics analyses shown in this paper that are during the left-to-right double support phase starting at 62% of the gait cycle, from 83 to 33 ms before left toe-off (Figure S5B).